Available online at www.sciencedirect.com

ScienceDirect

Ceramics International 40 (2014) 4811–4817

CERAMICS INTERNATIONAL

www.elsevier.com/locate/ceramint

Effect of nano-MgO on thermal and mechanical properties of aluminate cement composite thermal energy storage materials

Huiwen Yuan, Yu Shi, Zhongzi Xu*, Chunhua Lu**, Yaru Ni, Xianghui Lan

State key Laboratory of Materials-oriented Chemical Engineering, College of Materials Science and Engineering, Nanjing University of Technology, Nanjing 210009, China

Received 13 June 2013; received in revised form 9 September 2013; accepted 10 September 2013
Available online 17 September 2013

Abstract

Thermal and mechanical properties of high temperature aluminate cementitious thermal energy storage materials enriched with nano-MgO (NM) are investigated. According to the development of thermal storage materials and their application environment requirement in solar thermal power, the specimens were subjected to heating at 105, 350, and 900 °C. It was observed that the addition of NM provided a great improvement on the thermal properties of the composite pastes which were heated principally at 350 and 900 °C. When the NM content was 1 wt%, the thermal conductivities are 34.8% and 23.6% higher than that of pure paste at 350 and 900 °C, respectively. Meanwhile, at 2 wt% NM particles loading, the optimum value of volume heat capacity is obtained, which are 19.8% and 40.8% higher than that of pure paste at 350 and 900 °C, respectively. Moreover, compressive strength of the composite paste with 1 wt% NM presents approximately 30.5%, 27.8%, and 23.8% higher than that of pure paste at 105, 350, and 900 °C, respectively. XRD, TG-DSC, SEM, and MIP were used to characterize the phases, mass/heat changes, microstructure and pore distribution of the hardened cement pastes, respectively.

Keywords: C. Thermal/mechanical properties; Cementitious material; Thermal storage material

1. Introduction

Nowadays, solar thermal power has attracted growing research interest, which uses solar radiation as energy input without exhaust emission. Solar energy is a climate-affected energy source, and hence thermal energy storage (TES) is indispensable for its effective applications. Thermal energy storage (TES) systems can facilitate the integration of solar thermal power plants into the electrical grids by smoothing out fluctuations, thus avoiding instability problems and increasing electricity capacity [1–3]. In current solar thermal power plant projects, the molten salt storage technology is most commonly applied. However, this technology has the disadvantages of high freezing points and high investment costs. It is general knowledge that solid thermal storage material is carried out through inherent characteristics along with the temperature change, exhibiting non-toxicity and non-corrosiveness.

Cementitious/concrete material in solid thermal storage is regenerative storage concept with cyclic charging and discharging systems, meanwhile, it has the advantage of abundant source, low cost, and fine mechanical properties [3]. In addition, easy processing is also considered as one of the significant advantages. A first cementitious/concrete storage unit was tested successfully by the German Aerospace Center in Spain within a project funded by the German government [4]. Then one of the largest German building company, Ed. Züblin AG, joined the follow-up project which concentrated on cost reduction [5]. Aluminate cements have a correspondingly different chemistry to other cement such as Portland cements. Due to their higher cost, they do not compete directly with Portland cements. However, aluminate cement with special qualities such as excellent thermal resistance is of interest to study its novel function properties [6]. Such properties extend

*Corresponding author. Tel.: +86 25 83172128; fax: +86 25 83172128.
**Corresponding author. Tel.: +86 25 83587252; fax: +86 25 83587220.
E-mail addresses: yuanhuiwen722@126.com (H. Yuan), zzxu@njut.edu.cn (Z. Xu), chhlu@njut.edu.cn (C. Lu).

0272-8842/$ - see front matter © 2013 Published by Elsevier Ltd and Techna Group S.r.l.
http://dx.doi.org/10.1016/j.ceramint.2013.09.030

the thermal storage application field even at high temperature for aluminate cement materials. Some efforts are made to further optimize aluminate cementitious thermal storage materials and to improve the overall energy storage efficiencies [7–11].

Studies on nanoparticles in cementitious/concrete materials have started since the early 2000s [12–16]. Large surface area of nanoparticles to maximize the surface activity is highlighted all the time. The use of nanoparticles in cementitious/concretes materials significantly modifies their behavior not only in the fresh but also in the hardened conditions, as well as the physical/mechanical and microstructure development.

In this paper, we introduce nano-MgO (NM) into aluminate cementitious materials and prepare solar thermal storage composite materials. To date, few studies have been reported on thermal and mechanical performances in assessment of aluminate cementitious thermal energy materials. Heat-treatment was carried out at 105, 350, and 900 °C. Then thermal conductivity, volume heat capacity, and thermal expansion coefficient as well as compressive strength were provided in the paper. In addition, X-ray powder diffraction (XRD), Thermogravimetry-Differential Scanning Calorimeter (TG-DSC), Scanning Electron Microscopy (SEM) and Mercury Intrusion Porosimetry (MIP) were obtained to characterize the hydration phases, the mass/heat change, the microstructure, and the pore distribution of the hardened cement pastes, respectively.

2. Experimental

2.1. Materials

Aluminate cement used as cementing agent in this study was supplied by Zhengzhou Yuxiang Special Cement Plant in China. Table 1 presents the chemical compositions of this cement. Nano-MgO (NM) particles were supplied by Aladdin Reagent Database Inc., China. Fig. 1 illustrates the XRD pattern of NM particles consisted of mainly magnesia and a small amount of undecomposed $Mg(OH)_2$. Fig. 2 shows the TEM image of NM particles with an average particle size of 50 nm. High-performance polycarboxylate numbered for PCA-II supplied by Jiangsu Sobute New Materials Co., Ltd. in China was used for reducing water consumption and improving the dispersion of the fresh paste.

2.2. Sample preparation and curing

The control of water amount is particularly important in cement hydration process. The ratio of water to cement compound (the cement and NM particles) was chosen uniformly at 0.22. The six mix designs are designated as 0NM, 1NM, 2NM, 3NM, 4NM, and 5NM which represent mixing NM particles contents are 0 wt%, 10 wt%, 2 wt%, 3 wt%, 4 wt %, and 5 wt%, respectively. Each mixture was added with 1 wt% polycarboxylate. For better dispersion of the pastes, NM particles and polycarboxylate were first dispersed in water with mechanical stirring at a speed of 120 rpm for 5 min, and then the mixture was added to the cement powders for hydration reaction. The pastes cast for compressive strength, thermal conductivity, and thermal expansion coefficient were performed with molds of 20 mm × 20 mm × 20 mm, 48 mm × 20 mm × 80 mm, and 5 mm × 5 mm × 50 mm, respectively. The

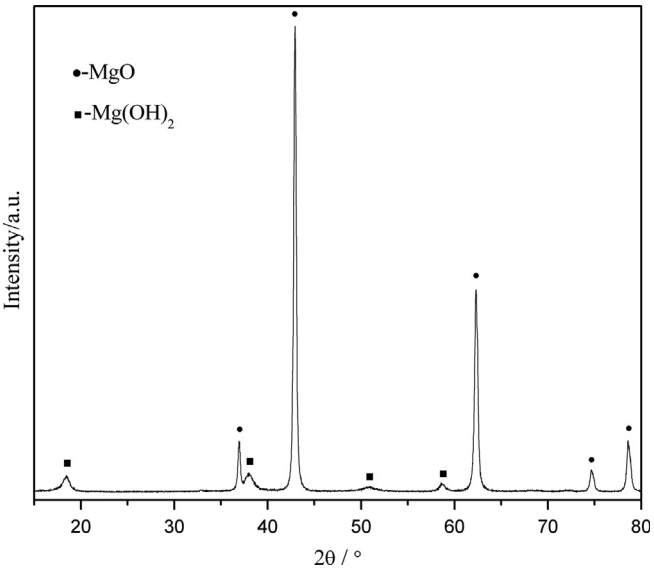

Fig. 1. XRD pattern of nano-MgO particles.

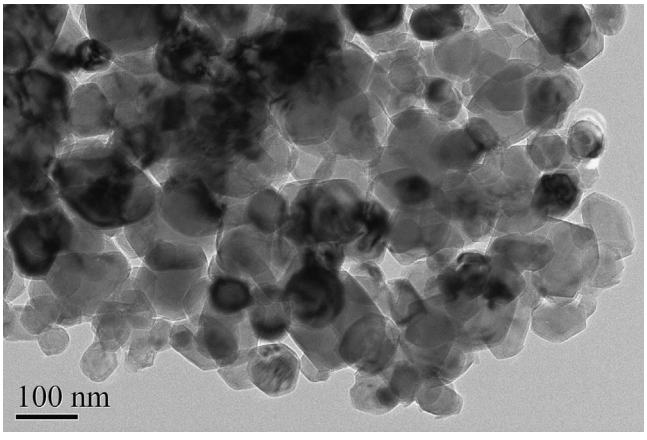

Fig. 2. TEM image of nano-MgO particles.

Table 1
Chemical compositions (wt%) of aluminate cement.

Materials	CaO	SiO_2	Al_2O_3	Fe_2O_3	R_2O	LOI
Aluminate cement	38.79	7.17	51.68	2.07	0.29	0.30

LOI: loss on ignition.

molds were covered with plastic wrap and moistened for 24 h. Then the specimens were demolded and cured in water at room temperature for 7 days. The selection of temperature depends strongly on the operation conditions of the respective application in solar thermal power plant. Otherwise, it is known that increasing the operating temperature of thermal storage material will improve the generation efficiency. In this paper, the specimens were heated at 105, 350, and 900 °C for 6 h.

2.3. Test procedures

Compressive strength was obtained by automatic pressure test machine (HualongWHY-200, Hualong Ltd., China) at a rate of 500 N s^{-1}. Thermal conductivity and volume heat capacity were measured by thermal conductivity constant tester (TPS2500, Hot Disk Ltd., Sweden) with Probe 5465 at 25 °C. For chemical analysis, the paste specimens are ground into powders with a maximum particle size of 80 μm. XRD (Rigaku D/Max-2500, Rigaku Ltd., Japan) was performed in the angular range 2θ from 15° to 60°, with Cu Kα radiation, a step size of 0.02°, and scan speed of 10 ° min. The measurement of TG-DSC (STA449C, Netzsch, Germany) was carried out in N_2 atmosphere at a heating rate of 20 °C min^{-1} ranging from room temperature to 900 °C. The morphologies were examined by Scanning Electron Microscopy (JSM-5900, JEOL, Japan). Then Mercury Intrusion Porosimetry (MIP) (PM-60-GT, Quantachrome Ltd., America) was used to obtain the pore distribution of the hardened cement pastes with the addition of NM.

3. Result and discussion

3.1. Thermal properties

3.1.1. Thermal conductivity

Table 2 shows thermal conductivity of aluminate cement pastes with different contents of NM after heat-treatment at 105, 350, and 900 °C, respectively. After the addition of NM, the thermal conductivity of the composite pastes after heat-treatment at 105 °C slightly decreases. It indicates that at this heat-treatment temperature the thermal conductivity is not obviously affected by the activated NM. Gratifying results have been obtained at the following two heat-treatment temperatures. When the NM content is 1 wt%, the thermal conductivity of composite paste after heat-treatment at 350 °C is up to 0.841 W/mK, which is 34.8% higher than that of pure paste. Then on further increasing heat-treatment temperature to 900 °C, the thermal conductivity of composite paste at 1 wt% NM particles loading indicates 23.6% higher than that of pure paste. Thus, it is worth noting that NM improves the thermal conductivity of the composite pastes especially at higher heat-treatment temperatures of 350 and 900 °C.

Table 2
Thermal conductivity of aluminate cement pastes with different contents of nano-MgO after heat-treatment at 105, 350, and 900 °C.

Sign	105 °C (W/mK)	350 °C (W/mK)	900 °C (W/mK)
0NM	1.187	0.621	0.542
1NM	1.184	0.841	0.670
2NM	1.098	0.630	0.603
3NM	1.101	0.627	0.595
4NM	1.120	0.643	0.616
5NM	1.103	0.642	0.616

3.1.2. Volume heat capacity

Table 3 shows similar tendency for volume heat capacity of pastes with different contents of NM after heat-treatment at 105, 350, and 900 °C. The volume heat capacity data of all the six samples is very close after heating at 105 °C, which indicates that at this temperature the activated NM does not strongly affect volume heat capacity either. The impact of NM on volume heat capacity appears at heat-treatment temperatures of 350 and 900 °C. The volume heat capacities of 1.935 MJ m^{-3} K^{-1} and 1.623 MJ m^{-3} K^{-1} are obtained at 2 wt% NM particles loading after heating at 350 and 900 °C, which are 19.8% and 40.8% higher than that of 0 NM, respectively.

3.1.3. Thermal stability

Thermal expansion coefficient curves of the pastes with different contents of NM are shown in Fig. 3. The measurement temperature ranges from 100 to 900 °C. After exposure to elevated temperature, the water vapor pressure in the paste will change. So the results were obtained after preheating in our experiment. It can be noted that when the temperature is up to 400 °C thermal expansion coefficient shows a slight fluctuation. Then the specimens still can keep stable ranging from 500 to 900 °C. The average value of thermal expansion coefficient is about 6×10^{-6} $°C^{-1}$. The difference in thermal expansion coefficient values of composite pastes enriched with NM is likely to be caused by the dehydration of the hydration products.

3.2. Mechanical properties

Compressive strength of aluminate cement pastes with different contents of NM after heat-treatment at 105, 350, and 900 °C is shown in Fig. 4. It can be noted that having more NM particles does not necessarily mean that it is better. The aluminate cement indicates rapid hardening and it is quite

Table 3
Volume heat capacity of pastes with different contents of nano-MgO after heat-treatment at 105 °C, 350 °C, and 900 °C.

Sign	105 °C (MJ m^{-3} K^{-1})	350 °C (MJ m^{-3} K^{-1})	900 °C (MJ m^{-3} K^{-1})
0NM	2.365	1.615	1.153
1NM	2.415	1.791	1.588
2NM	2.262	1.935	1.623
3NM	2.221	1.872	1.602
4NM	2.320	1.841	1.515
5NM	2.213	1.775	1.488

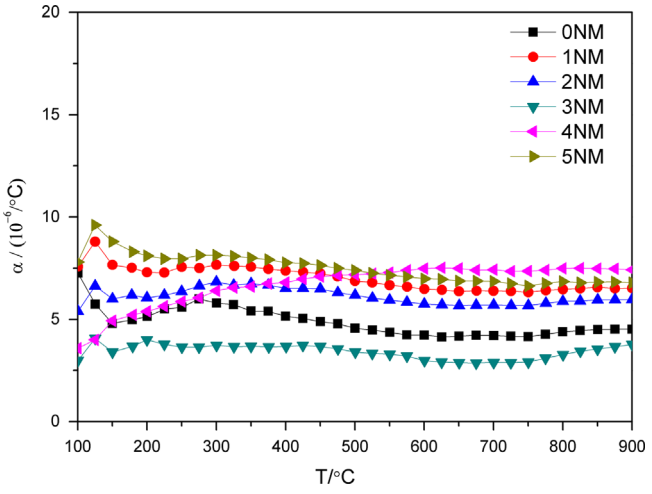

Fig. 3. Thermal expansion coefficient curves of the pastes with different contents of nano-MgO.

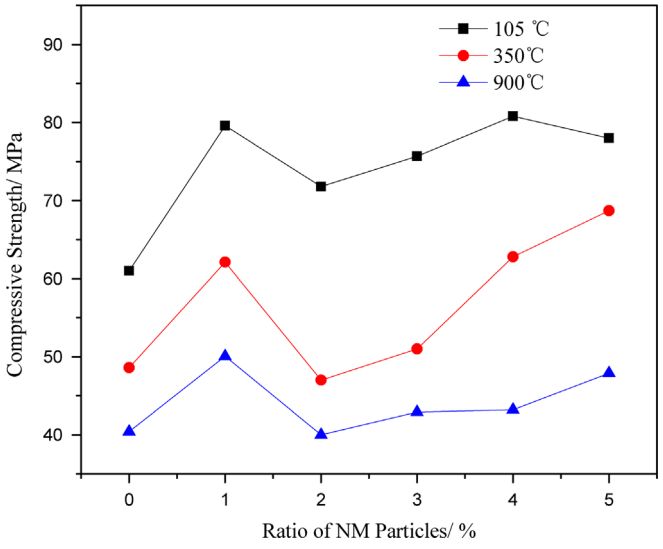

Fig. 4. Compressive strength of pastes with different contents of nano-MgO after heat-treatment at 105, 350, and 900 °C.

easy to obtain strengths in early age. The consequence of the rapid reaction is that the heat of hydration releases over a relatively short time. At the same time, the rapid temperature rise would not result in thermal cracking due to the special hydration products in aluminate cement. In the present paper, after heat-treatment at 105 °C, the compressive strength is greatly improved by addition of NM. Especially at 1 wt% NM particles loading, the compressive strength of the composite pastes is 30.5% higher than that of pure paste. As a matter of comparison, compressive strength of paste enriched with 1 wt % NM can reach 62.1 and 50.0 MPa at heat-treatment temperature of 350 and 900 °C, which is 27.8% and 23.8% higher than that of pure cement paste at the corresponding heat-treatment temperature, respectively. From Fig. 4 it also demonstrates that an obvious decrease of compressive strength occurred at the NM content of 2 wt%.

3.3. Characterization and analysis

3.3.1. X-ray diffraction analysis

Fig. 5 illustrates the XRD patterns of pastes enriched with different contents of NM after heat-treatment at 105, 350, and 900 °C. In the hydration process, the cement and NM (with water) tend to react and recombine to give a new mixture of phases that has the lowest energy-this is the stable phase assemblage. The activated NM changes the reaction environment due to the rearrangement of ions that needs to occur (nucleation). At all temperatures below 105 °C the stable hydration products of CA in pure paste are finally $3CaO \cdot Al_2O_3 \cdot 6H_2O$ (C_3AH_6-a form of hydrogarnet, JCPDS no. 77-240) and $Al_2O_3 \cdot 3H_2O$ (AH_3-poorly crystalline, JCPDS no. 29-41), the chemical reaction equation is shown as follows:

$$CA + 12H \rightarrow C_3AH_6 + 2AH_3 \quad (1)$$

As previously reported, the C_3AH_6 phase provides the main strength. A characteristic peak observed at $2\theta = 32.0^\circ$ pointed to the presence of C_3AH_6 phase. In this paper, after 7 d of curing in water at 25 °C and followed by heating for 24 h at 105 °C, various hydration products were formed such as C_3AH_6 and AH_3, as well as $Mg(OH)_2$ (MH, JCPDS no. 82-2454) formed by the reaction of NM particles with H_2O, as shown in Fig. 5(a). According to Deng et al. [17–20], MgO hydrates in solution of higher pH value to form MH with tiny crystals. From this, it can be inferred that as the NM particles are very fine and are mixed homogeneously within cement, tiny crystals of MH formed by the hydration of MgO may precipitate on the surface of the cement particles to form a 'protective layer'. Fig. 5(b) demonstrates that C_3AH_6 and AH_3 dehydrated after heating at 350 °C. And a new dehydrated product $3CaO \cdot Al_2O_3 \cdot SiO_2 \cdot 4H_2O$ (C_3ASH_4, JCPDS no. 32-151) was formed as well, whose characteristic peaks were observed at $2\theta = 17.6^\circ$, 27.1°, 32.6°, 40.1°, and 45.4°. Moreover, when the heat-treatment temperature was increased to 900 °C, a lot of phases began to decompose. In this case, MH dehydrated back to MgO, C_3ASH_4 dehydrated and decomposed into some anhydrous phases, and some more stable mineral phases began to appear, such as $CaO \cdot Al_2O_3$ (CA), $3CaO \cdot Al_2O_3$ (C_3A), and $12CaO \cdot 7Al_2O_3$ ($C_{12}A_7$), as shown in Fig. 5(c).

3.3.2. TG/DSC analysis

Fig. 6 shows the TG/DSC curves of pure paste and paste containing 1 wt% NM particles. The measurement temperature ranged from room temperature to 900 °C in nitrogen atmosphere, which was analyzed in conjunction with the XRD data. The hydration products in aluminate cement system are quite complex. The dehydration temperatures of AH_3 in pure paste are approximately at 282.2 °C [21,22]. As a matter of comparison, total weight loss of the paste enriched with 1 wt% NM was 2.1% higher than that of pure paste when the temperature ranged from 100 to 400 °C, which was caused by the decomposition of the chemically bound water in the paste.

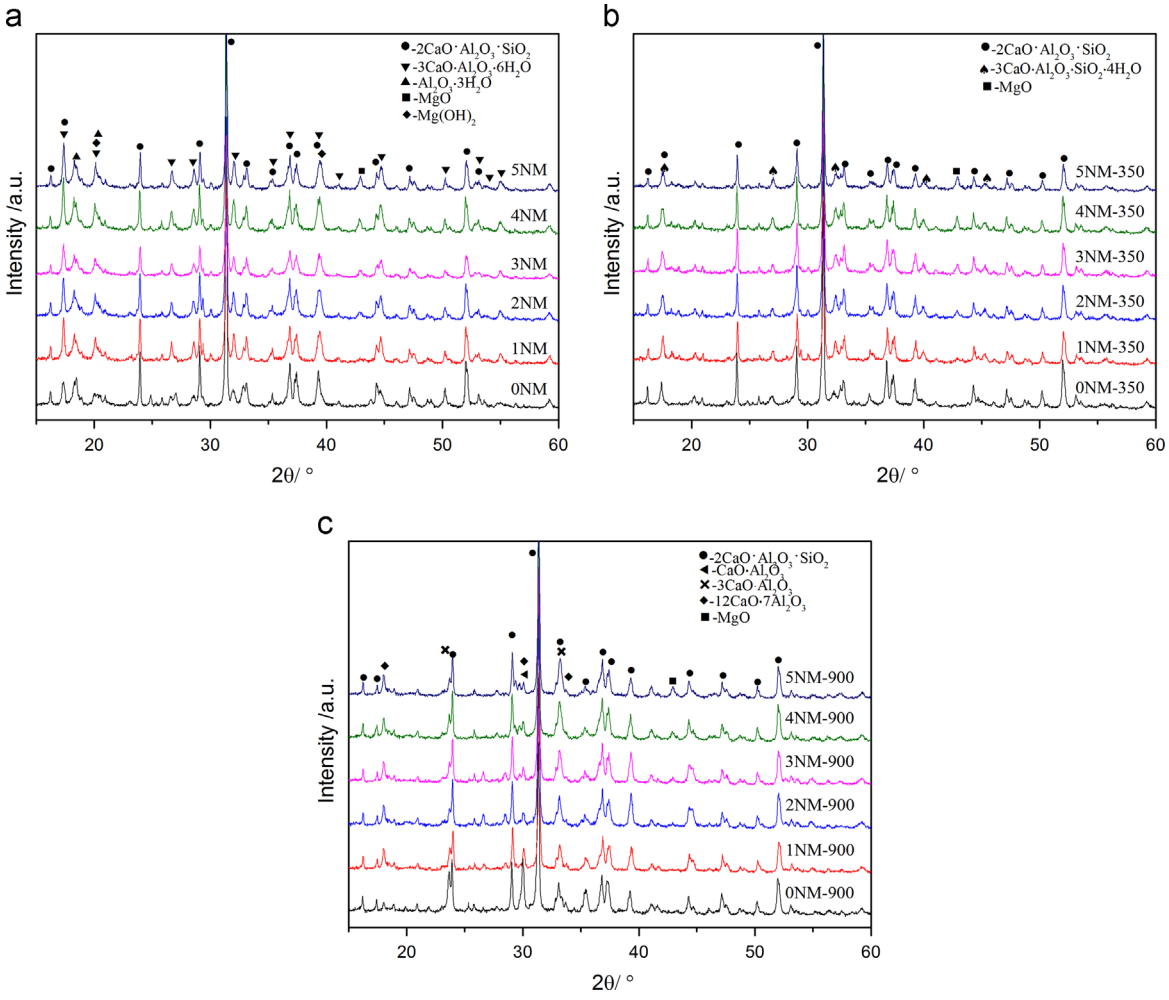

Fig. 5. XRD patterns of pastes with different contents of nano-MgO after heat-treatment at (a) 105 °C, (b) 350 °C, and (c) 900 °C.

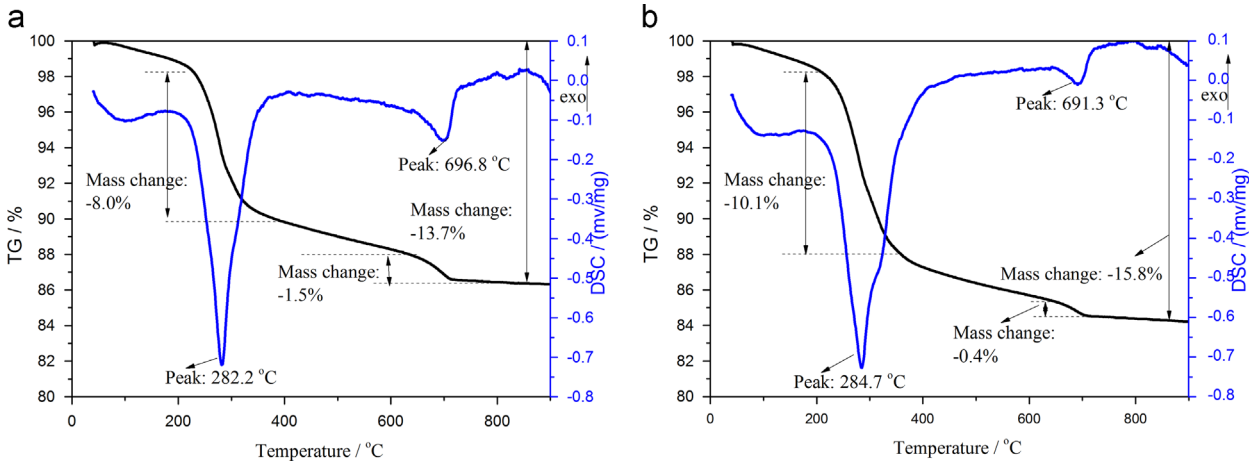

Fig. 6. TG/DSC curves of (a): pure paste; (b): paste containing 1 wt% nano-MgO particles.

Another observation on Fig. 6(a) and (b) was the weight loss difference associated with the characteristic peak around 690 °C. The composite pastes appeared to be only 0.4% weight loss corresponding to the dehydration of C_3ASH_4, while pure paste displayed 1.5% weight loss. The total weight losses of pure paste and the composite pastes were 13.7% and 15.8%, respectively.

3.3.3. SEM analysis

SEM images of pure paste and paste containing 1 wt% NM particles after heat-treatment at different temperatures are shown in Fig. 7. First observation of the pastes after heating at 105 °C indicated that besides some villus-like hydration products a lot of needle-like aluminate hydration products were formed in the composite paste after the addition of NM

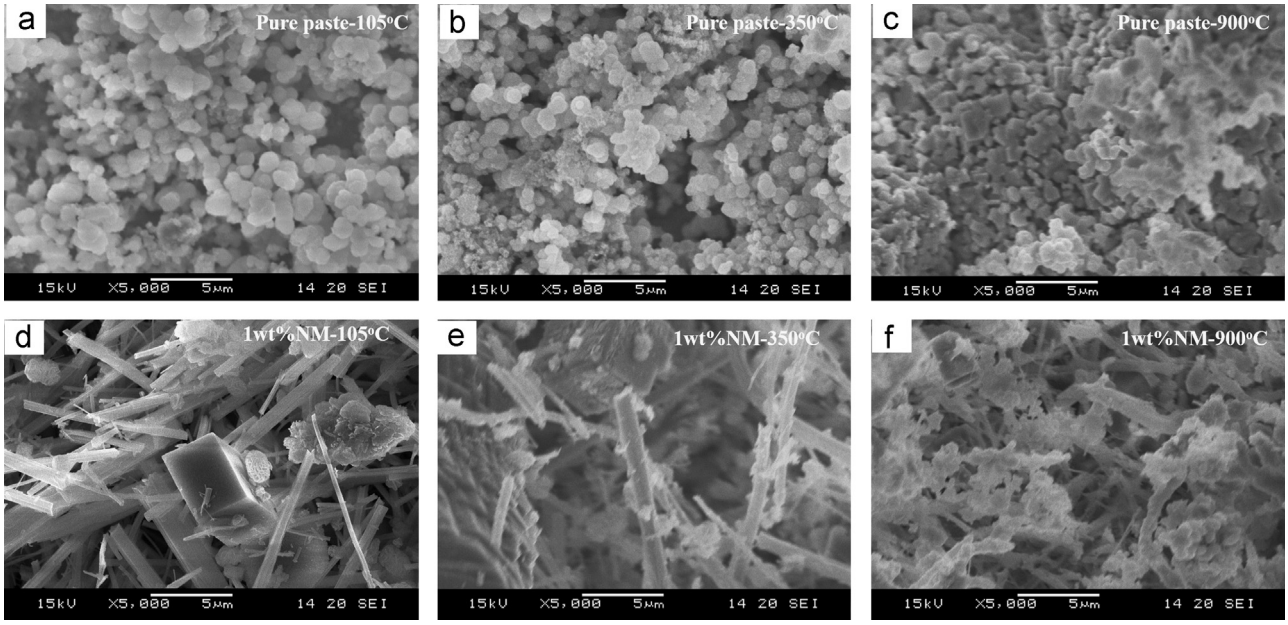

Fig. 7. SEM images of pure paste and paste containing 1 wt% nano-MgO particles after heat-treatment at 105 °C, 350 °C, and 900 °C.

particles. NM has resulted in the unusual features for the composite pastes compared with pure paste. Then the images of the pure paste and composite paste after heating at 350 °C are shown in Fig. 7(b) and (e), which was in accord with the XRD patterns shown in Fig. 5(b). The decomposition of some hydration products resulted in the decrease of the hydration particle in the pure paste and the cottony phenomenon of the needle-like hydration products in the composite paste enriched with NM particles. It is mainly due to the removal of some chemical bonding water from the hydration product. At the same time, the very scarce micro-cracks were present in the pastes after heat-treatment at 350 °C. Due to the high temperature up to 900 °C, macro-cracks were still present in the bulk specimen, which explained one of the reasons of the thermal and mechanical properties decrease reported above. Also, one notes the cottony phenomenon of the composite pastes enriched with NM is enhanced after heat-treatment at 900 °C, which shows higher densities than the pure paste (see Fig. 7(c)).

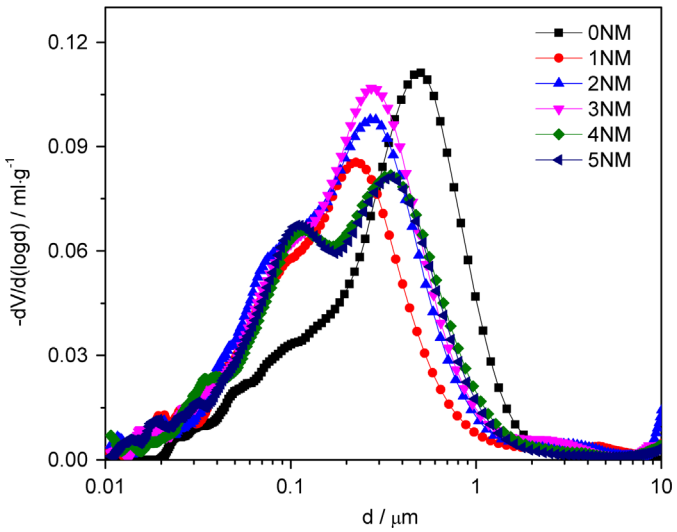

Fig. 8. MIP curves of pastes enriched with different contents of nano-MgO after heat-treatment at 105 °C.

3.3.4. Pore distribution analysis

Fig. 8 illustrates the influence of NM particles on pore distribution of the hardened cement composite pastes. As with Portland cement, and indeed any other porous material, the major factor related to strength is the porosity. In this paper, the pore distribution appears to become finer. This phenomenon indicates that after introducing NM the new hydration products has filled the larger pores effectively and has improved the structural stability as well. As shown in Fig. 8, the typical 'double peak' phenomenon gradually appeared as the addition of NM, especially at the amount of 4 wt% and 5 wt%. It indicated that the lowest porosity of the pastes occurred at 1 wt% NM content. With further increasing NM particles, the pore distribution began to increase again. Later, when the NM content was up to 4 wt% (or 5 wt%), a 'double peak' phenomenon turned up accompanying the reduction of pore size. It can be concluded that the influence of NM on the pore size of the cement pastes was a gradually process.

4. Conclusions

The addition of NM particles to aluminate cement paste significantly affected both thermal and mechanical properties, including thermal conductivity, volume heat capacity and compressive strength. Then the properties of the hydration pastes are shown to be highly sensitive to heat-treatment at different temperatures. The pore distribution of the composite paste was greatly optimized at 1 wt% NM particles loading and the typical 'double peak' phenomenon appeared.

When the NM content is 1 wt%, the thermal conductivity of composite paste heated at 350 °C is up to 0.841 W/mK, which is 34.8% higher than that of pure paste. At the same time, at 2 wt% NM particles loading, the optimum volume heat capacity is obtained, which is 40.8% higher than that of 0 NM after heating at 900 °C. Consequently, the matrix aluminate cementitious material with NM is available for future functional composite thermal storage materials. On the basis, the work of adding functional materials to improve thermal conductivity and volume heat capacity of heat-treated pastes still need to be carried out in the future.

Acknowledgments

The authors would like to express sincere thanks to Graduate Innovation Foundation of Jiangsu Province (CXLX11_0347), Priority Academic Program Development of Jiangsu Higher Education Institutions (PAPD) and the Independent Research Topics of State Key Laboratory of Materials-Oriented Chemical Engineering (ZK201211) for their financial support.

References

[1] Doerte Laing, Carsten Bahl, Thomas Bauer, et al., High-temperature solid-media thermal energy storage for solar thermal power plants, Proceedings of the IEEE 100 (2) (2012) 516–524.

[2] D. Laing, W.D. Steinmann, P. Viebahn, et al., Economic analysis and life cycle assessment of concrete thermal energy storage for parabolic trough power plants, Journal of Solar Energy Engineering—Transactions of the Asme 132 (4) (2010) 041013.

[3] Doerte Laing, Wolf-Dieter Steinmann, Michael Fib, et al., Solid media thermal storage development and analysis of modular storage operation concepts for parabolic trough power plants, Journal of Solar Energy Engineering 1 (011006) (2008) 011005130 1 (011006) (2008) 011005.

[4] Y. Tian, C.Y. Zhao, A review of solar collectors and thermal energy storage in solar thermal applications, Applied Energy 104 (2013) 538–553.

[5] Doerte Laing, Wolf-Dieter Steinmann, Rainer Tamme, et al., Solid media thermal storage for parabolic trough power plants, Solar Energy 80 (10) (2006) 1283–1289.

[6] Hajime Kinoshita, Paul Swift, Claire Utton, et al., Corrosion of aluminium metal in OPC- and CAC-based cement matrices, Cement and Concrete Research 50 (2013) 11–18.

[7] Hailong Li, Weilong Wang, Jinyue Yan, et al., Economic assessment of the mobilized thermal energy storage (M-TES) system for distributed heat supply, Applied Energy 104 (2013) 178–186.

[8] Huiwen Yuan, Chunhua Lu, Zhongzi Xu, et al., Mechanical and thermal properties of cement composite graphite for solar thermal storage materials, Solar energy 86 (11) (2012) 3227–3233.

[9] Hui Wen Yuan, Yu Shi, Chun Hua Lu, et al., Influence of polycarboxylate on thermal properties of cementitious solar thermal storage materials, in: Proceedings of the 2012 International Conference on Frontiers of Energy and Environmental Engineering: Taylor & Francis, Balkema, P.O. Box 447, Leiden, 2300 AK, Netherlands, 2013, pp. 89–93.

[10] Huiwen Yuan, Yu Shi, Zhongzi Xu, Chunhua Lu, Yaru Ni, Xianghui Lan, Influence of nano-ZrO_2 on the mechanical and thermal properties of high temperature cementitious thermal energy storage materials, Construction and Building Materials 48 (2013) 6–10.

[11] Emerson E. John, W. Micah Hale, R. Panneer Selvam, Development of a high performance concrete to store thermal energy for concentrating solar power plants, in: Proceedings of the ASME 2011 5th International Conference on Energy Sustainability, Aug. 7–10, Washington, DC., 2011.

[12] J.M. Fernández, A. Duran, I. Navarro-Blasco, et al., Influence of nanosilica and a polycarboxylate ether superplasticizer on the performance of lime mortars, Cement and Concrete Research 43 (2013) 12–24.

[13] M. Stefanidou, I. Papayianni, Influence of nano-SiO_2 on the Portland cement pastes, Composites: Part B 43 (6) (2012) 2706–2710.

[14] L. Senff, D. Hotza, S. Lucas, et al., Effect of nano-SiO_2 and nano-TiO_2 addition on the rheological behavior and the hardened properties of cement mortars, Materials Science and Engineering A 532 (2012) 354–361.

[15] Yibing Cai, Huizhen Ke, Ju Dong, et al., Effects of nano-SiO_2 on morphology, thermal energy storage, thermal stability, and combustion properties of electrospun lauric acid/PET ultrafine composite fibers as form-stable phase change materials, Applied Energy 88 (6) (2011) 2106–2112.

[16] G. Quercia, G. Hüsken, H.J.H. Brouwers, Water demand of amorphous nano silica and its impact on the workability of cement paste, Cement and Concrete Research 42 (2) (2012) 344–357.

[17] L. Mo, M. Deng, A. Wang, Effects of MgO-based expansive additive on compensating the shrinkage of cement paste under non-wet curing conditions, Cement and Concrete Composites 34 (2012) 377–383.

[18] Mo Liwu, Daman K. Panesar, Effects of accelerated carbonation on the microstructure of Portland cement pastes containing reactive MgO, Cement and Concrete Research 42 (2012) 769–777.

[19] Mo Liwu, Deng Min, Thermal behavior of cement matrix with high-volume mineral admixtures at early hydration age, Cement and Concrete Research 36 (2006) 1992–1998.

[20] Liwu Mo, Min Deng, Mingshu Tang, Effects of calcination condition on expansion property of MgO-type expansive agent used in cement-based materials, Cement and Concrete Research 40 (2010) 437–446.

[21] Dalun Ye, Jianhua Hu, The Handbook of Practical Inorganic Thermodynamic Data, Metallurgic Industry Press, Beijing, 2002.

[22] Nanru Yang, Haiwen Yue, The Handbook of Inorganic Metalloid Materials Atlas, Wuhan Industrial University Press, Wuhan, 2000.